RSA(EXT) 51

May 1994

Corrections to air kerma rate measurements of ^{125}I brachytherapy sources to free space conditions

D R Shipley and S Duane
Division of Radiation Science and Acoustics
National Physical Laboratory
Queens Road
Teddington
Middlesex
United Kingdom
TW11 0LW

ABSTRACT

Air kerma rate measurements have been made between 40 cm and 100 cm from one of a set of ^{125}I reference sources within the facilities of Amersham International plc. Monte Carlo techniques have been used to calculate the air kerma rate components over the same range of distances from this source. After comparing the calculated data with measurements, the compliance of the data with the inverse square law was investigated, and corrections were derived to obtain the air kerma rate at 1 m in free space from each source.

Simulations of the experimental setup with an isotropic monoenergetic point source close to the effective energy of ^{125}I were found to reproduce the air kerma rate measurements reasonably accurately, and indicated that the contribution due to scattered photons was significant. The overall correction (which is defined as the product of individual corrections for chamber size effect, air attenuation and radiation scatter) required to the inverse square law to obtain the air kerma rate at 1 m in free space was found to be 0.981, 0.984 and 0.980, respectively, for air kerma rate measurements at 40 cm, 60 cm and 100 cm from the ^{125}I reference source. The total uncertainty in these corrections was estimated to be 0.88% at the 1σ level.

ISSN 0955-9655

National Physical Laboratory
Teddington, Middlesex, UK, TW11 0LW

Approved on behalf of Chief Executive, NPL,
by Dr P Christmas, Acting Head, Division of Radiation Science and Acoustics.

CONTENTS

		Page
1	INTRODUCTION	
2	EXPERIMENTAL MEASUREMENTS	1
	2.1 SETUP	1
	2.2 PROCEDURE	2
	2.3 RESULTS	3
3	CALCULATION OF AIR KERMA	3
	3.1 THE EGS4 CODE SYSTEM	3
	3.2 METHOD OF CALCULATION	3
	3.3 RESULTS	4
4	DEVIATION FROM THE INVERSE SQUARE LAW	5
	4.1 OVERVIEW	5
	4.2 CORRECTIONS FOR CHAMBER SIZE AND AIR ATTENUATION	6
	4.2.1 Chamber size correction	6
	4.2.2 Air attenuation correction	7
	4.2.3 Comparison of corrected experimental data with calculation	7
	4.3 CORRECTION FOR RADIATION SCATTER	9
	4.4 OVERALL CORRECTION	10
5	UNCERTAINTIES	11
6	SUMMARY AND CONCLUSIONS	13
7	REFERENCES	15

ILLUSTRATIONS

Figure 1	Schematic diagrams showing (a) details of the ^{125}I source (and holder) and the secondary standard ionisation chamber, and (b) the location of the source and chamber within the experimental facility.	2
Figure 2	Variation of measured air kerma rate with distance from the ^{125}I source.	3
Figure 3	Variation of calculated total, primary and scattered air kerma (per initial decay) with distance from an isotropic monoenergetic 26 keV point source.	5
Figure 4	Variation of measured air kerma rate normalised to 1 m from the ^{125}I source, and calculated total and primary air rates normalised to 1 m from the 26 keV point source, after correcting for chamber size effect and air attenuation.	8
Figure 5	Least-square fits to the measured and calculated total air kerma rates (normalised to 1 m from the source).	8
Figure 6	Least-square fits to the measured and calculated total air kerma rates (normalised to 1 m) with a 27 keV monoenergetic point source.	10
Figure 7	Variation of the radiation scatter correction, and overall correction, with distance from the source.	11
Figure 8	Measured air kerma rate (normalised to 1 m from the source) after correcting for chamber size effect, air attenuation and radiation scatter.	12
Figure A1	Spherical kerma detector.	18
Figure A2	Cubic kerma detector.	19

TABLES

Table I Corrections for chamber size effect, air attenuation and radiation scatter required to obtain the air kerma rate in free space at 1 m for the set of ^{125}I reference sources. 14

Table II Air kerma rates at 1 m in free space obtained by Medi-Physics, Amersham International and NPL for the set of ^{125}I reference sources. 15

APPENDICES

APPENDIX 1 Kerma at a point and averaged over a sphere and over a cube of finite size 17

1 INTRODUCTION

Brachytherapy is the treatment of diseased tissue using small X-ray and γ-ray emitting radionuclide sources that are inserted either directly in, or in close proximity to, the affected volume. The brachytherapy sources that tend to be most commonly used are ^{137}Cs and ^{192}Ir, and they are available in a wide variety of geometric forms (for example, pins, wires, beads etc). In recent years, there has been a demand for improved accuracy in their calibration and better quality control. In the United Kingdom, the traceability route for the calibration of brachytherapy sources, supplied by Amersham International plc, to national standards at the NPL has been in place for many years[1]. Such calibrations have depended on the ionometric comparison of source output with a set of ^{60}Co reference sources (which had been calibrated by comparison with an NPL secondary standard ^{226}Ra source and, in one case, by dissolution and absolute counting). The validity of these calibrations was later established by direct measurements of the exposure rate from such sources using a secondary standard protection-level ionisation chamber[2]. These measurements were later repeated[3] and extended to include the radionuclide ^{192}Ir, and to take account of the recommendation by the British Committee on Radiation Units and Measurements (BCRU) that brachytherapy sources be specified in terms of air kerma rate (instead of exposure rate) at 1 m in free space[4].

At present, the range of brachytherapy source standardisations undertaken by the NPL is limited to the sources mentioned above, but it is intended to extend this range to include the low energy radionuclide ^{125}I. A knowledge of the air kerma rate at 1 m in free space is therefore required to characterise this source[(1)]. The first part of this report describes air kerma rate measurements that were performed at different distances from an ^{125}I reference source. The method used to calculate the air kerma rate components over the same range of distances from the source is then discussed. The calculated results are compared with experiment, in the second part of the report, and the compliance of the data with the inverse square law is investigated. Corrections to the measured data are then derived to obtain the air kerma rate in free space at 1 m from each of the set of reference sources.

2 EXPERIMENTAL MEASUREMENTS

2.1 SETUP

The experimental setup for the measurement of air kerma rate under minimal scattering conditions at different distances from reference brachytherapy sources is shown in Figure 1(a). The sources were placed in a paper vee located on a small Perspex support which was attached to the end of a hollow Tufnol pillar approximately 4 m in length. A calibrated NE 2551/1 secondary standard protection-level ionisation chamber, attached to the end of another hollow Tufnol pillar of similar length, was positioned at a horizontal distance of between 40 cm and 100 cm from the source. For extra stability, the two vertical pillars were clamped together using a horizontal Tufnol rod approximately 50 cm below the source. The chamber had been calibrated at NPL in low energy X-ray beams and the calibration factor used was the mean of those obtained at 24 and 33 keV in which range the chamber response is essentially energy-independent. X-rays in the region of 4 keV are totally absorbed in the chamber wall.

To enable measurements to be performed under conditions of minimal scattering, the apparatus was setup within the facilities of Amersham International at the Harwell Laboratory. This facility is essentially a large hanger having a floor area of approximately 25 m × 15 m and a height of 15 m. The apparatus was mounted approximately 3 m above the floor near one corner of the facility, close to a concrete block house (see Figure 1(b)).

---

(1) Principal X-ray emissions are at 27 keV with subsidiary emissions at 32 and 35 keV and at 3–5 keV together with fluorescence X-rays from the Ti encapsulation at 4.5 keV.

(a)

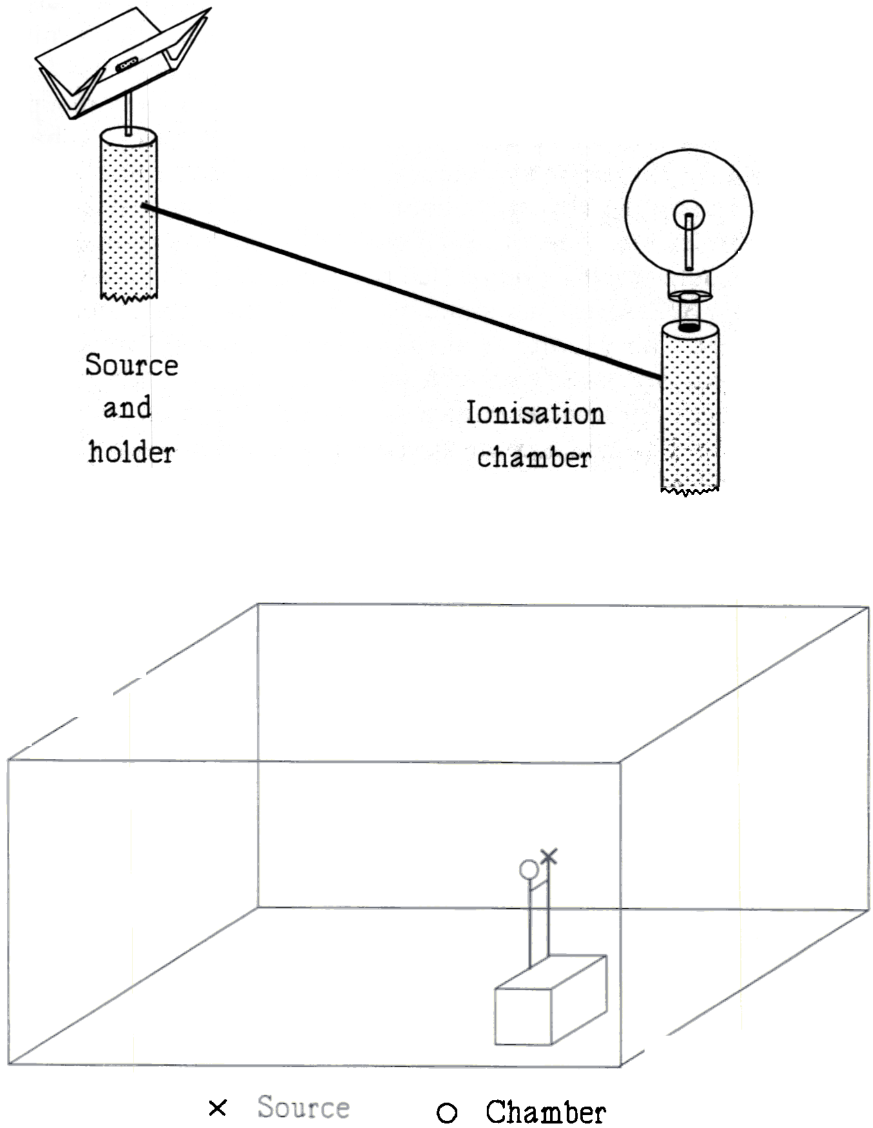

Figure 1 Schematic diagrams showing (a) details of the ^{125}I source (and holder) and the secondary standard ionisation chamber, and (b) the location of the source and chamber within the experimental facility.

2.2 PROCEDURE

An ^{125}I reference brachytherapy source (Source No: R2024K) with a nominal activity of 1.35 GBq (36.5 mCi) was used for the measurements. The source consists of a welded titanium capsule, approximately 4 mm in length and 1 mm in diameter, containing ^{125}I absorbed on three spheres of anion exchange resin (Amersham code IMC 6702). Air kerma rate measurements, carried out by Williams and Bass[5], were made at various distances between 40 cm and 100 cm from the source over a period of 2 days. Background measurements were also made and their mean subtracted from each source reading. The atmospheric pressure and ambient temperature were recorded for each measurement and all readings were corrected to 101.3 kPa and 20°C. Since the half-life of ^{125}I is quite short (59.4 days), the time of each measurement was also noted and a source decay correction applied.

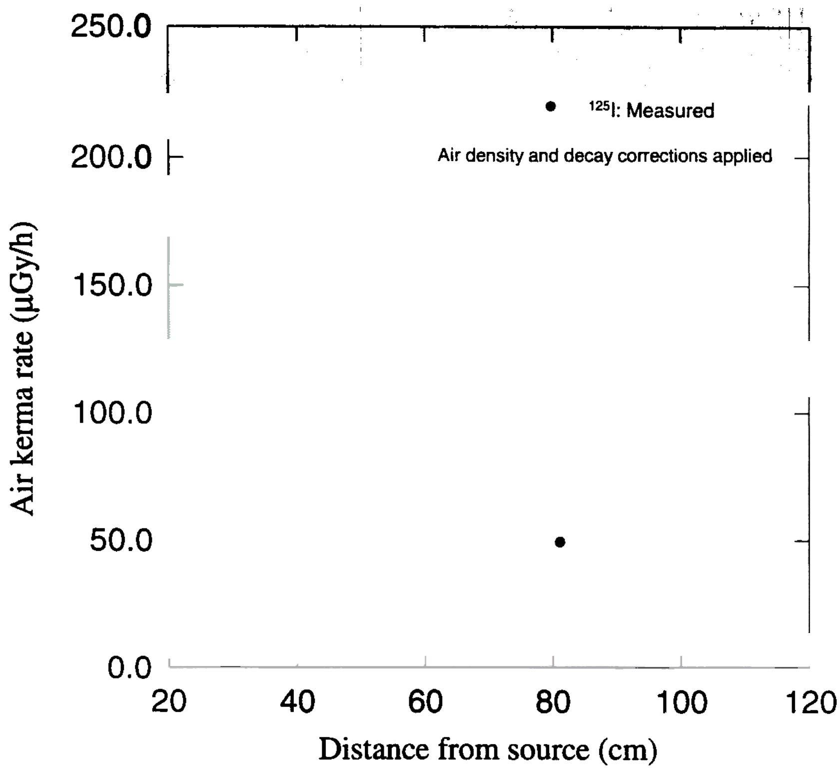

Figure 2 Variation of measured air kerma rate with distance from the ^{125}I source.

2.3 RESULTS

The results of the measurements are shown in Figure 2 after applying the relevant chamber calibration and measuring assembly range factors. The standard error of the mean for each set of readings was better than 0.2% (1σ). The measurement at 97 cm from the source was repeated, and the difference between the two mean values was 0.6%. The measurement uncertainty was therefore assumed to be 0.6% (1σ) at all distances. The compliance of the measured data with the inverse-square law will be investigated later in Section 4.

3 CALCULATION OF AIR KERMA

3.1 THE EGS4 CODE SYSTEM

Most of the calculations described in this report were carried out using the EGS4[(2)] code system[6]. These codes form a general purpose package for the Monte Carlo simulation of the coupled transport of electrons and photons in an arbitrary geometry for particles with energies ranging from a few keV to several TeV. The package, used in conjunction with a user-written code, calculates the development of an electron-photon cascade from a single incident electron or photon, and transports each and every particle through the geometry until it reaches a predefined energy cutoff or discard boundary. Electron-photon transport can be simulated in any of 100 elements or mixture of these elements, or any compound. The associated package PEGS4[(3)], documented by Nelson et al.[6], is used to generate datasets of the required materials for subsequent use by EGS4.

3.2 METHOD OF CALCULATION

An EGS4 user code XYZKER (Version 1.10) was developed to calculate the variation of air

---

(2) Electron Gamma Shower version 4

(3) Preprocessor for EGS4.

kerma rate with distance from the ^{125}I brachytherapy source (taking into account photon attenuation and scatter). This code calculates the air kerma (per initial decay) averaged over 10 cm cubes centred at horizontal distances of between 40 cm and 100 cm from the source[(4)]. The kerma due to primary, scattered and Rayleigh scattered photons was also determined in each scoring region (along with their sum as a check on energy conservation). To reduce the complexity of the code, the source capsule was replaced with an isotropic monoenergetic point source close to the effective energy of ^{125}I, that is 26 keV[(5)]. This is a reasonable approximation since the actual source capsule has a very thin wall (≤ 0.05 mm of titanium), changing the effective energy only very slightly, and the size of the capsule is small compared to the distance between the source and the region of interest. The walls, floor and ceiling of the experimental facility (which were assumed to be made of concrete) and the concrete blockhouse were included in the simulations since the mean free path of 26 keV photons in air (~19 m) is of the same order of magnitude as the hanger dimensions. No attempt was made to simulate the effect of the source holder and chamber and their supports.

The coding for the simulation geometry and the material definitions were checked using the program KGTEST3 (Version 1.00). This code first places point sources at random in each geometric region and then stores the coordinates of the point of intersection of a randomly-directed 'ray' with the nearest boundary. The outline of each region is then revealed when the points are plotted with an interactive graphics package. The points from regions containing the same material can also be grouped together to enable the distribution of a given material throughout the geometry to be verified.

The datasets required by EGS4 for all the materials in the simulation geometry were generated using PEGS4. In each case, the option to include Rayleigh (coherent) scattering data in the output was also selected since these interactions are significant at these photon energies.

The EGS4 transport parameters were set to the following values for all regions in the geometry. The minimum (total) electron energy required for explicit δ-ray production, AE, was set to 0.512 MeV, and the minimum (total) energy for electron transport, ECUT, was set to 1.511 MeV. AP and PCUT, the photon equivalents of AE and ECUT, were both set to 0.001 MeV. With these cutoffs, there is no electron transport in the simulations since the electrons are discarded immediately after they are produced. This has no significant effect on the air kerma in each scoring region and greatly reduces the computation time per initial decay.

The photon fluence calculations were performed on an Elonex PC-466 PC system using Lahey F77L-EM/32 Fortran (Version 5.01). With the above transport parameters, approximately one hundred million initial photon decays (at a rate of 6.9 M decays per hour) were required to calculate the air kerma averaged over a 10 cm cube to a statistical uncertainty at the 1σ level of 0.1% at 40 cm from the source, and 0.3% at 100 cm from the source.

3.3 RESULTS

The variation of calculated air kerma (per initial decay) with distance from the source is shown in Figure 3. As can be seen, the total and primary air kerma decrease with distance in a similar way to the measured air kerma rate (Figure 2). The scattered air kerma is significant at these distances, forming a greater proportion of the total kerma further from

---

(4) The user code XYZKER actually calculates the *collision* kerma in an XYZ geometry. The collision kerma in air, however, is numerically equal to the total kerma for photon energies less than 1 MeV.

(5) It was found that the experimental measurements are most accurately reproduced when the isotropic monoenergetic point source has an energy of 26 keV, even though the effective energy of ^{125}I is closer to 27 keV.

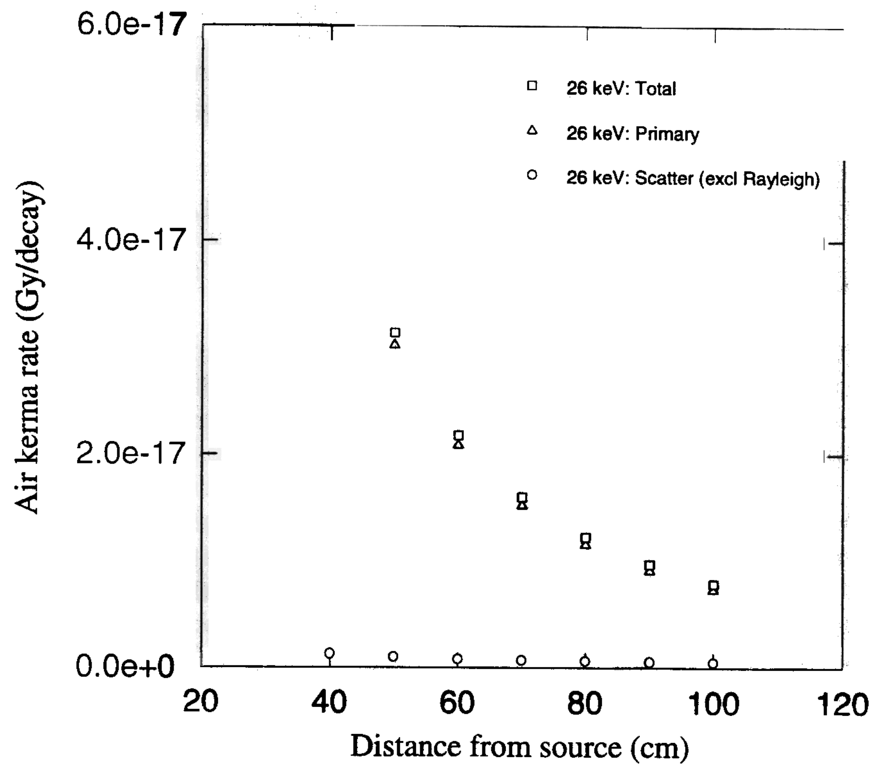

Figure 3 Variation of calculated total, primary and scattered air kerma (per initial decay) with distance from an isotropic monoenergetic 26 keV point source.

the source. Approximately 10% of the total scatter is due to Rayleigh-scattered photons. The calculations therefore show that the experimental facility is not quite scatter-free and that corrections may be required to the measured air kerma values to account for this scattered radiation (see Section 4.3).

4 DEVIATION FROM THE INVERSE SQUARE LAW

4.1 OVERVIEW

The aim of this project was to determine the air kerma rate at 1 m from a reference ^{125}I brachytherapy source under scatter-free conditions. In order to obtain the air kerma rate constant from the measured data, however, a number of corrections are required. A chamber of finite size is used in the experimental measurements, and hence the effective point of measurement is likely to be closer to the source than the geometric centre of the chamber. A correction is therefore needed to account for this chamber size effect. An air attenuation correction is also required since the attenuation of the photon fluence between the source and point of measurement is significant at low energies. After allowing for the chamber size effect and air attenuation, the air kerma rate at a given distance from the source should be inversely proportional to the square of the distance from the source, under scatter-free conditions. However, the simulations of the experimental setup have shown that a significant proportion of the measured kerma is due to scattered radiation, and so a further correction to account for this radiation may also needed.

The methods used to determine the corrections for chamber size effect and air attenuation in the experimental measurements are discussed in Section 4.2. The correction for radiation scatter is obtained from the simulation results and is discussed in Section 4.3. Although a correction for scatter is required, the correction is small enough that scatter can be neglected in the evaluation of the correction for air attenuation. Likewise, attenuation and scatter are both neglected in the derivation of the chamber size correction. In other words, the combined correction, for attenuation, scatter and chamber size effect, is treated to first order only.

In all cases, the source has been assumed to be point-like. This is a good approximation since the source-chamber distances used in this work are very large compared to the physical size of the source capsule.

4.2 CORRECTIONS FOR CHAMBER SIZE AND AIR ATTENUATION

4.2.1 Chamber size correction

The NE 2551/1 ionisation chamber used in the experimental measurements has a spherical carbon fibre shell (approximately 0.3 mm thick), with an internal diameter of 183 mm, and a spherical collecting electrode of diameter 38 mm. Since the diameter of the collecting volume is of the same order of magnitude as the smallest source-chamber distances used in the measurements, the air kerma rate can vary significantly across the chamber volume due to the diverging photon field. Hence the effective point of measurement and geometric centre of the chamber will not coincide. The effective point of measurement of a spherical chamber has been considered by Kondo and Randolph[7], but their analysis assumes that all the secondary electrons originate from the chamber walls. In this case, with a maximum photon energy of 26 keV, the range of secondary electrons in air (~1.3 cm) is much smaller than the size of the collecting volume and hence the measured ionisation is practically all due to electrons generated by photon scattering inside the chamber volume (that is, the chamber acts as a photon detector).

The chamber was calibrated against the primary standard free air chamber at a distance of 2 m from a point source. Any perturbation of the photon fluence by the chamber wall and stem therefore forms part of the measured calibration factor. If we assume that this perturbation is independent of distance from the source, then the calibration factor will be valid for distances closer to the source provided one allows for any change in the effective point of measurement. For a spherical chamber of radius r_{ch} centred at a distance R_0 from a point source, the air kerma rate $\dot{K}_{ch}$ averaged over the chamber volume, in the absence of attenuation and scatter, may be estimated using the expression (from equation (A9) in Appendix 1):

$$\dot{K}_{ch} = \dot{N}(E) \frac{E}{4\pi\left(R_0^2 - \frac{r_{ch}^2}{5}\right)} \left(\frac{\mu_{en}}{\rho}\right)_{E,air} \quad \text{for } E \leq 1.0\,\text{MeV},\ r_{ch} < 0.5\,R_0 \qquad (1)$$

where $\dot{N}(E)$ is the rate at which photons cross a sphere of radius R_0 centred at the point source, and $(\mu_{en}/\rho)_{E,air}$ is the mass-energy absorption coefficient for air at a photon energy E. The air kerma rate $\dot{K}_{pt}$ at a distance R_0 from the point source is given by (from equation (A6) in Appendix 1):

$$\dot{K}_{pt} = \dot{N}(E) \frac{E}{4\pi R_0^2} \left(\frac{\mu_{en}}{\rho}\right)_{E,air} \quad \text{for } E \leq 1.0\,\text{MeV} \qquad (2)$$

The correction k_{ch} required to obtain the actual air kerma rate from the measured air kerma rate at a distance R_0 from a point source, using a spherical chamber of radius r_{ch}, is therefore given by the ratio of these expressions:

$$k_{ch} = 1 - \frac{r_{ch}^2}{5R_0^2} \quad \text{for } r_{ch} < 0.5\,R_0 \qquad (3)$$

The correction k_{ch} is less than unity since the effective point of measurement is closer to the point source than the actual measurement point giving a slightly higher reading for the air kerma rate than required. For the NE 2551/1 ionisation chamber used in the experimental measurements, k_{ch} ranges from 0.9895 at 40 cm from the source to 0.9983 at 100 cm from the source. These chamber size corrections are within ~0.1% of the corrections used by Read et al.[2] for a similar protection-level secondary standard ionisation chamber in the calibration of ^{60}Co, ^{226}Ra and ^{137}Cs sources. Corrections equal to one-half those predicted by Kondo and Randolph were used in that case to produce the best fit to the experimental data, but the full correction was used when the measurements were repeated[3].

The correction to account for the finite size of the cubic scoring regions, k_{sr}, used in the calculation of air kerma, is derived in a similar way (using equations (A6) and (A15) in Appendix 1) and is given by:

$$k_{sr} = 1 - \frac{d^2}{3R_0^2} \qquad \text{for } d < 0.3\,R_0 \tag{4}$$

where R_0 is the distance from the point source to the centre of the scoring region (of side $2d$). k_{sr} has a value of 0.9948 at 40 cm from the source and 0.9992 at 100 cm from the source for the 10 cm cubes used in the simulations.

Air attenuation correction

The air kerma rate $\dot{K}$ due to primary photons at a distance R_0 from a point source may be expressed in the form:

$$\dot{K} = \frac{\dot{K}_0 \exp(-\mu_{air} R_0)}{R_0^2} \tag{5}$$

where $\dot{K}_0$ is the air kerma rate at 1 m in free space and μ_{air} is the narrow-beam attenuation coefficient for air. The air attenuation correction, k_{att}, that accounts for the attenuation of the photon beam by the intervening air is therefore:

$$k_{att} = \exp(\mu_{air} R_0) \tag{6}$$

These expressions ignore the energy-absorption buildup factor[8] which takes into account the contribution of scattered photons in $\dot{K}$ (reducing the effective attenuation of the photon beam). In the present analysis, this is included in the radiation scatter correction (Section 4.3). The mass-attenuation coefficients for air, $(\mu/\rho)_{air}$, were obtained in this work using the computer program XCOM[9]. This program generates cross sections and mass attenuation coefficients for any element, compound or mixture at energies between 1 keV and 100 GeV. For 26 keV photons, $(\mu/\rho)_{air}$ is 0.4346 cm^2 g^{-1} which gives a value for k_{att} of 1.0212 at 40 cm from the source and 1.0538 at 100 cm from the source.

Comparison of corrected experimental data with calculation

Figure 4 shows the variation of air kerma rate normalised to 1 m from the source after correcting for chamber size effect (k_{ch}) and air attenuation (k_{att}). The normalisation to 1 m is obtained in each case by multiplying the corrected air kerma rate by the square of the measurement distance (in metres). Under scatter-free conditions, the corrected air kerma rate is inversely proportional to the square of the measurement distance and thus the normalised air kerma rate should be independent of distance. However, as can be seen from the plot, the normalised air kerma rate increases with distance from the source indicating that radiation scatter is significant and must be corrected for in the experimental measurements (see Section 4.3).

The variation of calculated total and primary air kerma rates, normalised to 1 m from the 26 keV point source, is also shown in Figure 4, after correcting for scoring region size (k_{sr}) and air attenuation (k_{att}). The error bars indicate the statistical uncertainty at the 1σ level. These air kerma rates (in units of µGy h^{-1}) were derived from the simulation results (in units

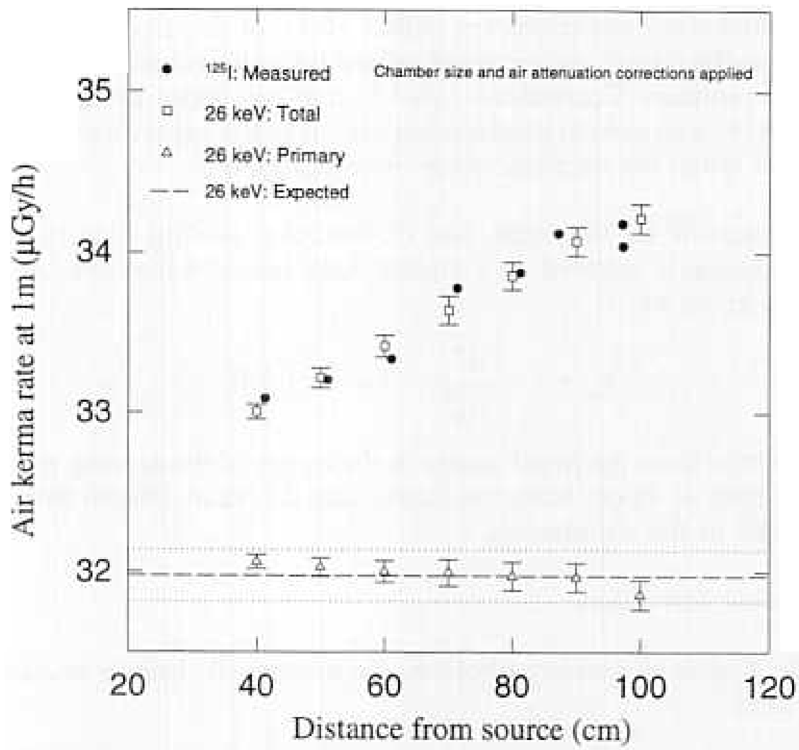

Figure 4 Variation of measured air kerma rate normalised to 1 m from the ^{125}I source, and calculated total and primary air rates normalised to 1 m from the 26 keV point source, after correcting for chamber size effect and air attenuation. The expected value for the air kerma rate at 1 m from the 26 keV source is also shown with the two lines on either side representing the estimated uncertainty in this value.

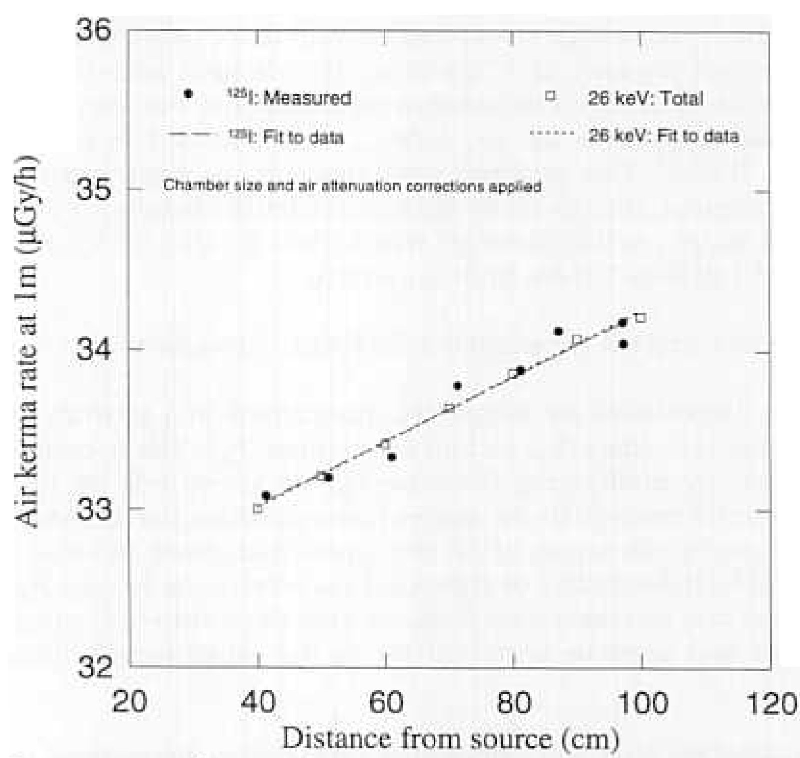

Figure 5 Least-square fits to the measured and calculated total air kerma rates (normalised to 1 m from the source).

of Gy per initial decay) by assuming the source had a nominal activity of 1.15 GBq (31.0 mCi). This is equal to the estimated activity of the ^{125}I source at the reference time used in the measurements (1.04 GBq) multiplied by a factor equal to 1.098. This normalisation factor is required to match calculation with experiment since the activity of the source is not accurately known.

As can be seen from Figure 4, the calculated total air kerma rate (normalised to 1 m) increases with distance from the source in a similar way to the experimental data. The normalised primary air kerma rate, however, is more or less independent of distance from the source, as one would expect, confirming that scattered photons are responsible for the observed variation of the normalised total air kerma rate with distance. The dashed line in the figure indicates the direct value[(6)] for the air kerma rate at 1 m from a 26 keV monoenergetic isotropic point source (in the absence of attenuation and scatter), that is, 31.98 ± 0.16 (1σ) μGy h^{-1} using the mass-energy absorption coefficient data of Hubbell[10]. The primary air kerma rate at each distance agrees with this value to within 1-2σ indicating that the calculations of air kerma rate are reliable.

Figure 5 shows the measured and calculated air kerma rates (normalised to 1 m) after applying a linear least-squares fit to the data. For the ^{125}I source, the gradient and intercept of the regression line are (2.02 ± 0.20) × 10^{-2} μGy h^{-1} cm^{-1} and 32.22 ± 0.15 μGy h^{-1} respectively, with uncertainties quoted at the 1σ level. For the 26 keV point source, the gradient and intercept are (2.06 ± 0.05) × 10^{-2} μGy h^{-1} cm^{-1} and 32.19 ± 0.03 μGy h^{-1} respectively. As can be seen, the gradients and intercepts of the regression lines agree to within 1σ, indicating that the experimental data can be reproduced very closely by replacing the ^{125}I source capsule and holder with a 26 keV isotropic monoenergetic point source.

The calculated air kerma rates were found to be quite sensitive to the energy of the point source. With a 27 keV point source, the gradients of the regression lines applied to the normalised calculated and experimental air kerma rates are (2.38 ± 0.06) × 10^{-2} μGy h^{-1} cm^{-1} and (1.90 ± 0.20) × 10^{-2} μGy h^{-1} cm^{-1} respectively (see Figure 6). In this case, the gradients differ by more than 2σ. This is also true with a 25 keV point source, where the gradients were found to differ by ~2σ in the opposite direction. The small change in the gradient of the experimental data is due to the different air attenuation corrections being used. A point source with an energy of 26 keV was therefore taken as an optimal choice to reproduce the experimental data.

4.3 CORRECTION FOR RADIATION SCATTER

The discussion in the previous section has shown that experimental measurements with the ^{125}I source can be accurately reproduced using Monte Carlo techniques. One can therefore use the simulation results to estimate the correction required to account for radiation scatter in the measurements. If $\dot{K}_{pr}$ is the kerma rate due to primary photons at a point in air at a given distance from the source, and $\dot{K}_{sc}$ is the kerma rate due to scattered photons at that point (whatever their origin), then the total air kerma rate $\dot{K}$ at the point is given by:

$$\dot{K} = \dot{K}_{pr} + \dot{K}_{sc} \tag{7}$$

It then follows that the correction factor k_{sc} required to account for scattered radiation at the point in air has the form:

---

(6) The direct calculation of air kerma rate at 1 m from the 26 keV point source assumes an activity of 1.15 GBq (equal to the nominal activity of the ^{125}I source multiplied by the normalisation factor). The uncertainty quoted in this value is due to the 0.5% estimated uncertainty in the interpolation of the mass-energy absorption coefficient data, which is indicated in the figure by the two dotted lines on either side of the expected value. The uncertainty in the actual data (~2%) is not included in this value.

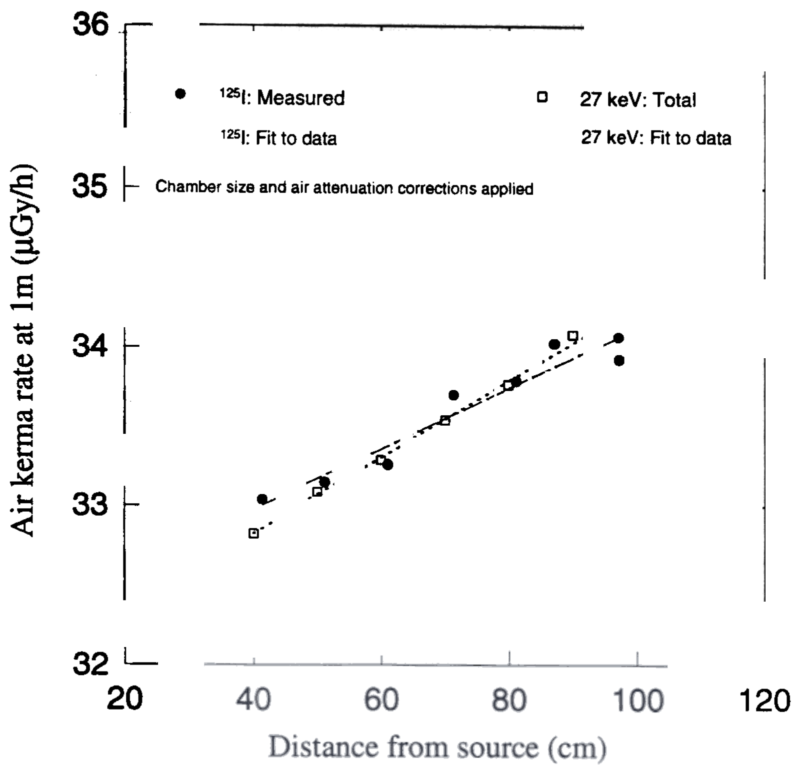

Figure 6 Least-square fits to the measured and calculated total air kerma rates (normalised to 1 m) with a 27 keV monoenergetic point source.

$$k_{sc} \quad \frac{\dot{K}_{pr}}{\dot{K}_{pr} + \dot{K}_{sc}} \quad \frac{\dot{K}_{pr}}{\dot{K}} \quad (< 1) \tag{8}$$

In this work, the values for k_{sc} required to correct the experimental data were estimated from the ratio of primary and total air kerma rates calculated at different distances from the 26 keV point source. The variation of k_{sc} with distance from the source is shown in Figure 7. The gradient and intercept of the least-squares line applied to the data are $(-6.643 \pm 0.047) \times 10^{-4}$ cm^{-1} and 0.9977 ± 0.0003 respectively. The standard error in the gradient is much smaller here, compared to the values obtained earlier (Section 4.2.3), since the correlation between the primary and total air kerma rates in equation (8) has been exploited in the simulations. The least-squares fit was then evaluated at each measurement distance to obtain the required corrections to the experimental data. The correction k_{sc} ranges from 0.9714 at 40 cm from the source to 0.9312 at 100 cm from the source.

4.4 OVERALL CORRECTION

The overall correction factor k_{ov} at each measurement distance, defined as the product of the corrections for chamber size effect, air attenuation and radiation scatter ($k_{ch} \times k_{att} \times k_{sc}$), is also shown in Figure 7. The equation of the curve is given by:

$$k_{ov} = \left(1 - \frac{r_{ch}^2}{5R_0^2}\right) \exp(\mu_{air} R_0)(a_{sc} + b_{sc} R_0 \qquad \text{for } r_{ch} < 0.5\, R_0 \tag{9}$$

where a_{sc} and b_{sc} are respectively the intercept and gradient of the least-squares line applied to the data for the radiation scatter correction (see Section 4.3). Using this equation, the overall correction at 1 m from the source is 0.9797. As can be seen from the figure, k_{ov} does not vary greatly over the range of distances considered indicating that the two largest corrections, for radiation scatter and air attenuation, almost cancel out. The correction for

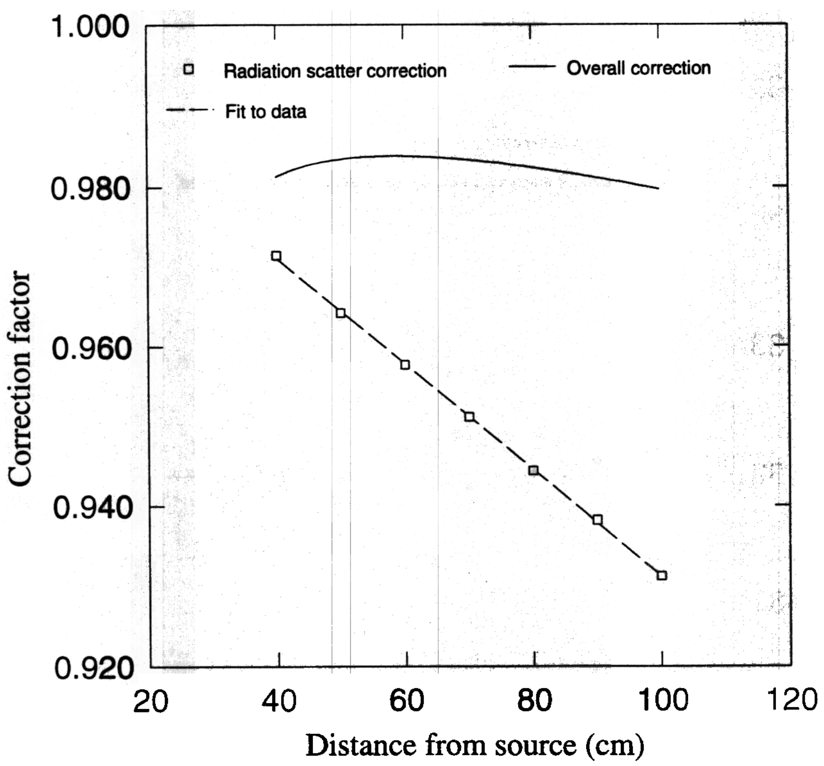

Figure 7 Variation of the radiation scatter correction, and overall correction, with distance from the source.

chamber size effect, although much smaller in magnitude than the other two corrections, therefore has a significant effect on the overall correction factor and should not be ignored. For comparison, with a 25 keV point source, the overall correction factor at 1 m is 0.9855. In this case, the correction is closer to unity (by ~0.6%), primarily due to the larger air attenuation correction at this energy.

The variation with distance of the measured air kerma rate normalised to 1 m from the source after correcting for chamber size effect, air attenuation and radiation scatter is shown in Figure 8. The expected value for the air kerma rate at 1 m from the 26 keV point source (in the absence of attenuation and scatter) is also shown. As can be seen, the corrected air kerma rates now satisfy the inverse-square law and are in close agreement with the expected value.

5 UNCERTAINTIES

The random and systematic uncertainties in the determination of the overall correction factor for measurements with the ^{125}I source will be considered in this section. As discussed in Section 2.3, the random uncertainty in the source measurements was estimated from the spread of two separate measurements of air kerma rate at 97 cm from the source, that is 0.6% at the 1σ level. This value seems reasonable since it is roughly equal to the maximum deviation of each measured air kerma rate (after correction) from the expected value, as shown in Figure 8.

There are also a number of systematic uncertainties associated with the individual corrections that make up the overall correction factor. In the determination of the correction for finite chamber size, the ionisation chamber used in the measurements was replaced by a sphere of the same radius, and the assumption was made that the perturbation of the photon fluence by the chamber cavity was independent of distance from the source (since the chamber is normally calibrated at 2 m from a point source). It is difficult to determine exactly how these

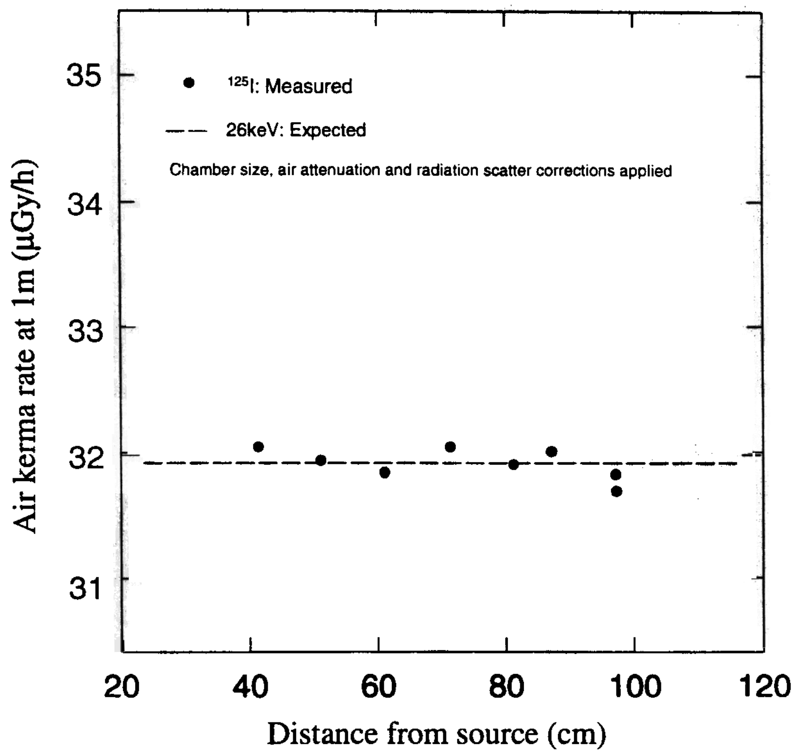

Figure 8 Measured air kerma rate (normalised to 1 m from the source) after correcting for chamber size effect, air attenuation and radiation scatter. The expected value for the air kerma rate at 1 m from a 26 keV source is also shown.

assumptions will affect the calculated chamber size corrections without carrying out a more detailed analysis. However, a value of 0.2% at the 1σ level was thought to be a reasonable estimate of the systematic uncertainty in this correction. This is probably a conservative estimate since the correction is itself quite small (0.2–1.0%).

The major source of uncertainty in the correction for air attenuation is associated with the values used for the mass attenuation coefficient for air. In this work, the computer program XCOM was used to generate the required attenuation coefficients (which, apart from one or two small differences, are virtually identical to those tabulated by Hubbell[10] and Cullen et al.[11]). At photon energies of around 25 keV in air, approximately 45% of photons undergo incoherent (Compton) scattering and 45% undergo photoelectric absorption (with the remainder scattering coherently). The cross section for incoherent scattering is accurately known and thus the uncertainty in the corresponding partial attenuation coefficient is small. However, this not the case with photoelectric absorption, where the quoted uncertainty in the interaction cross section at these photon energies is typically 2% (Hubbell[10]). With approximately half of the photons undergoing photoelectric absorption, the estimated uncertainty in the mass attenuation coefficient data used in this work is 1%. The systematic uncertainty in the air attenuation corrections, which lie in the range 4.6–7.8%, is therefore at most 0.08% at the 2σ level.

The corrections for radiation scatter were derived from the ratio of primary and total air kerma rates calculated at different distances from a 26 keV point source. There are several factors contributing to the uncertainty in the calculation of the air kerma rate. There is an estimated 0.5% uncertainty in the interpolation of the mass-energy absorption coefficient data, used to derive the air kerma rate, as well as an estimated 1% uncertainty in the coefficients themselves (presumed to be the same as that for the mass attenuation coefficient data). Since the primary and total air kerma rates are correlated in the simulations, these uncertainties mostly cancel out when taking the ratio, and is estimated to be ~0.08% (2σ) at worst. The statistical uncertainties in the calculated air kerma rates, however, appear as a systematic uncertainty in the radiation scatter correction. This systematic uncertainty is at most 0.07% at the 1σ level (obtained by taking the largest statistical uncertainties in the scatter and total air kerma rates in quadrature).

The energy of the monoenergetic point source used to try and reproduce the experimental data is another source of uncertainty in the calculation of air kerma rate. Although the experimental data can be reproduced reasonably accurately using a 26 keV point source (with an appropriate normalisation factor), a change of 1 keV in the energy of the source changes the overall correction by 0.6% (Section 4.4). Since the random uncertainties in the experimental data (and thus the standard error in the gradient of the corresponding regression line) are quite large, a reasonable estimate for the systematic uncertainty in the overall correction factor due to this uncertainty in the point source energy is therefore 0.6% at the 1σ level.

The estimated total uncertainty in the overall correction factor is therefore 0.88% at the 1σ level, obtained by taking the random and systematic uncertainties in quadrature. This is dominated by the 0.6% random uncertainty in the experimental measurements, and the 0.6% uncertainty in the choice of the effective point source energy.

6 SUMMARY AND CONCLUSIONS

The measurements of air kerma rate at distances between 40 cm and 100 cm from the ^{125}I brachytherapy source can be reproduced reasonably accurately by simulating the experimental setup with a 26 keV monoenergetic isotropic point source. These simulations indicate that, after correcting for chamber size effects and air attenuation, there is a significant contribution to the measured air kerma rate by scattered photons, even though the measurements have been performed under minimal scattering conditions. The primary air kerma rates, also determined in the simulations, obey the inverse square law (after correction) and, when normalised to a distance of 1 m from the source, are in close agreement with the expected value at this distance. This indicates that the simulations of the experimental setup are reliable.

Table I summarises the corrections for chamber size effect (k_{ch}), air attenuation (k_{att}) and radiation scatter (k_{sc}) required to obtain the air kerma rate at 1 m in free space from the measured air kerma rate, for the ^{125}I brachytherapy source considered in this work (Source number: R2024K), and for other ^{125}I sources of similar construction. One should note that the corrections for air attenuation and radiation scatter are large but change the air kerma rate in opposite directions. The chamber size correction, although much smaller in magnitude, will therefore have a significant effect on the air kerma rate and should not be ignored. The overall corrections (defined as the product of k_{ch}, k_{att} and k_{sc}) required to the inverse square law for source number R2024K are 0.9813, 0.9838 and 0.9797 respectively at 40 cm, 60 cm and 100 cm from the source. The estimated total uncertainty in this correction is 0.88% at the 1σ level and hence is just about significant at the 95% confidence level (taken to be 2σ).

For completion, the corrected air kerma rate values for the set of ^{125}I sources are compared in Table II with values supplied by Amersham International and Medi-Physics Inc. (USA) for the same reference date (8 December 1992)[12]. As can be seen, the NPL values agree with the uncorrected Amersham values to within ~2%. The Medi-Physics values for this batch of ^{125}I seeds, however, are at least 10% higher than both the NPL and Amersham values. This is probably due to the inclusion of 4.5 keV fluorescence X-rays (from the Ti encapsulation) in the NIST calibrated ^{125}I seed[13].

Table I Corrections for chamber size effect, air attenuation and radiation scatter required to obtain the air kerma rate in free space at 1 m for the set of ^{125}I reference sources.

Source serial number	Distance (cm)	Measured reading (μGy h^{-1})	k_{ch}	k_{att}	k_{sc}	Corrected reading at 1 m (μGy h^{-1})
R2024K	41.406	190.71	0.9902	1.0219	0.9702	32.10
	51.162	124.29	0.9936	1.0272	0.9637	32.00
	61.141	86.75	0.9955	1.0325	0.9571	31.90
	71.399	64.04	0.9967	1.0381	0.9503	32.10
	81.312	49.23	0.9975	1.0435	0.9437	31.97
	87.199	42.97	0.9978	1.0467	0.9398	32.07
	97.231	34.42	0.9982	1.0522	0.9331	31.89
	97.302	33.23	0.9982	1.0523	0.9330	31.76
R2029I	97.223	29.04	0.9982	1.0522	0.9331	26.90
R2032L	97.223	13.52	0.9982	1.0522	0.9331	12.53
R2018C	97.223	10.68	0.9982	1.0522	0.9331	9.90
R2025E	97.223	27.81	0.9982	1.0522	0.9331	25.76
	97.223	27.92	0.9982	1.0522	0.9331	25.87
R2018B	97.223	10.80	0.9982	1.0522	0.9331	10.01
	97.223	10.77	0.9982	1.0522	0.9331	9.98

Table II Air kerma rates at 1 m in free space obtained by Medi-Physics, Amersham International and NPL for the set of ^{125}I reference sources.

Source serial number	Air kerma rate at 1 m in free space (μGy h^{-1})			Ratio NPL/Amersham
	Medi-Physics†	Amersham‡	NPL	
R2024K	35.75	31.13	31.83	1.022
R2029I	30.37	26.57	26.90	1.012
R2032L	14.21	12.28	12.53	1.020
R2018C	11.27	9.73	9.90	1.017
R2025E	28.90	25.23	25.81	1.023
R2018B	11.27	9.92	9.99	1.007

† Measurements made in a re-entrant ionisation chamber against a NIST (NBS) calibrated ^{125}I seed[12].

‡ Measurements made inside a concrete cell using an NPL calibrated thin-window ionisation chamber (NET 2575). No corrections have been applied for air attenuation and scatter, and chamber size effect[12].

7 REFERENCES

1 ROSSITER, M.J. The traceability of brachytherapy sources supplied by Amersham International. *Br. J. Radiol.*, 1990, **63**, 663.

READ, L.R., BURNS, J.E. and LIQUORISH, R.A.C. Exposure-rate calibration of small radioactive sources of ^{60}Co, ^{226}Ra and ^{137}Cs. *Int. J. Appl. Radiat. Isot.*, 1978, **29**, 21–27.

3 ROSSITER, M.J., WILLIAMS, T.T. and BASS, G.A. Air kerma rate calibrations of small sources of ^{60}Co, ^{137}Cs, ^{226}Ra and ^{192}Ir. *Phys. Med. Biol.*, 1991, **36**, 279–284.

4 BCRU. Specification of brachytherapy sources. *Br. J. Radiol.*, 1984, **57**, 941–942.

5 WILLIAMS, T.T. and BASS, G.A. Private communication. 1993.

6 NELSON, W.R., HIRAYAMA, H. and ROGERS, D.W.O. The EGS4 code system. *Report SLAC-265*, Stanford Linear Accelerator Center, Stanford, CA 94305, 1985.

7 KONDO, S. and RANDOLPH, M.L. Effect of finite size of ionisation chambers on measurements of small photon sources. *Radiat. Res.*, 1960, **13**, 37–60.

8 BERGER, M.J. *J. nucl. Med.*, 1968, **9**, Suppl. No. 1

9 BERGER, M.J. and HUBBELL, J.H. XCOM: Photon cross sections on a personal computer. *Report NBSIR 87-3597*, National Bureau of Standards, Gaithersburg, MD 20899, 1987.

10 HUBBELL, J.H. Photon mass attenuation and energy-absorption coefficients from 1 keV to 20 MeV. *Int. J. Appl. Radiat. Isot.*, 1982, **33**, 1269–1290.

11 CULLEN, D.E., CHEN, M.H., HUBBELL, J.H., PERKINS, S.T., PLECHATY, E.F., RATHKOPF, J.A. and SCOFIELD, J.H. Tables and graphs of photon-interaction cross sections from 10 eV to 100 GeV derived from the LLNL evaluated photon data library (EPDL). *Report UCRL-50400, Vol. 6, Part A, Rev. 4,* Lawrence Livermore National Laboratory, Livermore, CA 94551, 1989.

12 LIQUORISH, R.A.C. Private communication. 1993.

13 KUBO, H. Exposure contribution from Ti *K* X-rays produced in the titanium capsule of the clinical ^{125}I seed. *Med. Phys.*,1985, **12**, 215–220.

APPENDIX 1 Kerma at a point and averaged over a sphere and over a cube of finite size

An expression for the air kerma from a point source is used in this appendix to determine the response of a spherical and a cubic 'kerma detector'.

A1.1 KERMA AT A POINT

If $\Psi(E,R)$ is the photon energy fluence at a distance R from an isotropic monoenergetic point source in air, the kerma K is given by:

$$K = \Psi(E,R)\left(\frac{\mu_{tr}}{\rho}\right)_{E,air} \qquad \text{(A1)}$$

where $(\mu_{tr}/\rho)_{E,air}$ is the mass-energy transfer coefficient for air at the photon energy E. In terms of the photon fluence $\Phi(E,R)$:

$$K = E\,\Phi(E,R)\left(\frac{\mu_{tr}}{\rho}\right)_{E,air}$$

In the absence of air attenuation and scatter, the photon fluence $\Phi_0(E,R)$ would take the form:

$$\Phi_0(E,R) = \frac{N(E)}{4\pi R^2}$$

where $N(E)$ is the number of photons emitted by the source, and so the kerma K_0 in the absence of attenuation and scatter would be:

$$K_0 = E\,\frac{N(E)}{4\pi R^2}\left(\frac{\mu_{tr}}{\rho}\right)_{E,air}$$

The mass-energy transfer coefficient is related to the mass-energy absorption coefficient for air, $(\mu_{en}/\rho)_{E,air}$, by:

$$\left(\frac{\mu_{en}}{\rho}\right)_{E,air} = (1-g_{air})\left(\frac{\mu_{tr}}{\rho}\right)_{E,air} \qquad \text{(A5)}$$

where g_{air} represents the average fraction of secondary electron energy that is lost in radiative interactions along its path in air. For photon energies less than about 1.0 MeV in air, g_{air} is negligible and $(\mu_{tr}/\rho)_{E,air}$ can be replaced by $(\mu_{en}/\rho)_{E,air}$. K_0 then becomes:

$$K_0 = E\,\frac{N(E)}{4\pi R^2}\left(\frac{\mu_{en}}{\rho}\right)_{E,air} \qquad \text{for } E \le 1.0\,\text{MeV}$$

Naturally, the kerma in free space decreases with the square of the distance from the source (the inverse-square law).

A1.2 KERMA IN A SPHERE OF FINITE SIZE

Consider a spherical kerma detector, of radius r_S, centred at point P_0 at a distance R_0 from the source (Figure A1). When r_S has the same order of magnitude as R_0, the kerma at different points within the spherical volume will vary significantly due to the diverging photon fluence. In particular, the region closer to the point source will contribute more to the average kerma than the region further away from the source. As a result, the effective centre of the sphere and the geometric centre will not coincide. The average kerma K_{sph} in the sphere can be written as an integral over the volume of the sphere:

$$K_{sph} = \frac{3}{4\pi r_S^3}\int_{sphere} E\,\frac{N(E)}{4\pi R^2}\left(\frac{\mu_{en}}{\rho}\right)_{E,air} d^3R \qquad \text{for } E \le 1.0\,\text{MeV}$$

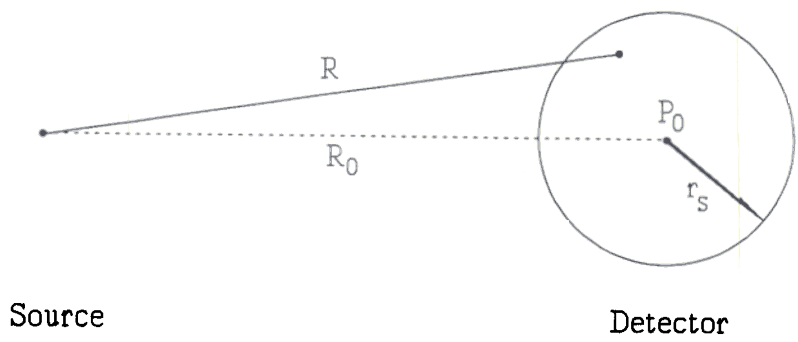

Figure A1 Spherical kerma detector.

Evaluating this integral[7] leads to the expression:

$$K_{sph} = E\,\frac{N(E)}{4\pi}\left(\frac{\mu_{en}}{\rho}\right)_{E,air}\frac{1}{R_0^2}\left(1+\frac{1}{5R_0^2}r_S^2+\frac{3}{35R_0^4}r_S^4+O(r_S^6)\right) \tag{A8}$$

If $r_S < 0.5R_0$, the second order is sufficient for most kerma calculations (the fourth order term providing a correction smaller than 1%), in which case:

$$K_{sph} \approx E\,\frac{N(E)}{4\pi\left(R_0^2-\frac{r_S^2}{5}\right)}\left(\frac{\mu_{en}}{\rho}\right)_{E,air} \qquad \text{for } E \le 1.0\,\text{MeV},\ r_S < 0.5R_0$$

So a spherical kerma detector of finite size has an effective centre displaced somewhat towards the source compared to the geometric centre. The displacement Δ varies with distance R_0 such that:

$$(R_0-\Delta)^2 \approx R_0^2-\frac{r_S^2}{5} \tag{A10}$$

Solving for Δ gives:

$$\Delta = R_0-\sqrt{R_0^{\,2}-\frac{r_S^2}{5}} \tag{A11}$$

which can be simplified using a series expansion to:

$$\Delta \approx \frac{r_S^2}{10\,R_0} \tag{A12}$$

As one would expect, there is no displacement when r_S=0.

A1.3 KERMA IN A CUBE OF FINITE SIZE

The response of a cubic kerma detector is determined in a same way as for a spherical detector (Section A1.2). For a cube of side $2d$ centered at point P_0 in homogeneous air at a distance R_0 from the point source (Figure A2), the kerma K_{cube} averaged over the volume of the cube is:

[7] One of the three integrals can be done analytically, the other two require series expansions.

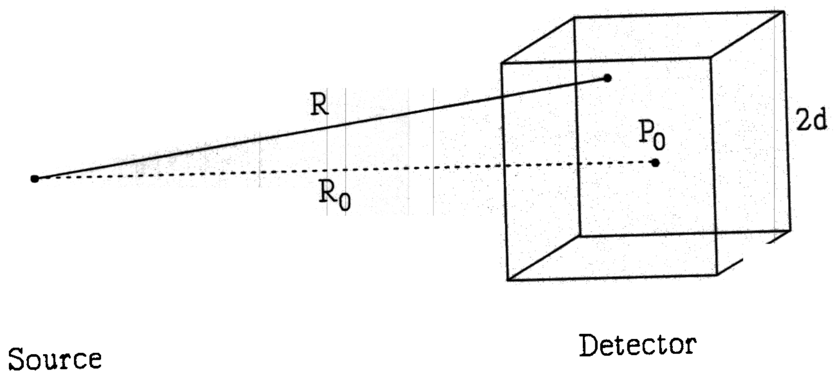

Figure A2 Cubic kerma detector.

$$K_{\text{cube}} = \frac{1}{8d^3} \int_{\text{cube}} E \frac{N(E)}{4\pi R^2} \left(\frac{\mu_{\text{en}}}{\rho}\right)_{E,\text{air}} d^3R \qquad \text{for } E \leq 1.0\,\text{MeV} \tag{A13}$$

Evaluating K_{cube} using series expansions gives:

$$= E \frac{N(E)}{4\pi} \left(\frac{\mu_{\text{en}}}{\rho}\right)_{E,\text{air}} \frac{1}{R_0^2} \left(1 + \frac{1}{3R_0^2} d^2 - \frac{3}{5R_0^4} d^4 + O(d^6)\right) \tag{A14}$$

and, in the case when $d < 0.3R_0$, this can be re-expressed in the form:

$$K_{\text{cube}} \approx E \frac{N(E)}{4\pi\left(R_0^2 - \frac{d^2}{3}\right)} \left(\frac{\mu_{\text{en}}}{\rho}\right)_{E,\text{air}} \qquad \text{for } E \leq 1.0\,\text{MeV},\ d < 0.3\,R_0 \tag{A15}$$

This expression is only slightly different to the kerma averaged over a sphere (equation (A9)), and matches the kerma at a point (equation (A6)) when d is set to zero. The displacement Δ of the effective centre of the cubic detector from its geometric centre is:

$$\Delta \approx \frac{d^2}{6R_0} \tag{A16}$$

which is obtained in the same way as before.